Quaternary Science Reviews 248 (2020) 106572

Contents lists available at ScienceDirect

Quaternary Science Reviews

journal homepage: www.elsevier.com/locate/quascirev

Neoglacial increase in high-magnitude glacial lake outburst flood frequency, upper Baker River, Chilean Patagonia (47°S)

Elke Vandekerkhove [a, *], Sebastien Bertrand [a], Dmitri Mauquoy [b], Dave McWethy [c], Brian Reid [d], Sarah Stammen [a], Krystyna M. Saunders [e], Fernando Torrejón [f]

[a] Renard Centre of Marine Geology (RCMG), Department of Geology, Ghent University, Belgium
[b] School of Geosciences, University of Aberdeen, Aberdeen, United Kingdom
[c] Department of Earth Sciences, Montana State University, Bozeman, USA
[d] Centro de Investigación en Ecosistemas de la Patagonia (CIEP), Universidad Austral de Chile, Coyhaique, Chile
[e] Australian Nuclear Science and Technology Organisation, Lucas Heights, Australia
[f] Centro EULA, Universidad de Concepción, Concepción, Chile

A R T I C L E I N F O

Article history:
Received 15 April 2020
Received in revised form
24 July 2020
Accepted 29 August 2020
Available online xxx

Keywords:
Paleohydrology
Paleofloods
GLOF
Floodplain
Loss-on-ignition
Neoglaciation

A B S T R A C T

Glacial Lake Outburst Floods (GLOFs) constitute a major threat in glacierized regions. Despite a recent increase in the size and number of glacial lakes worldwide, there is only limited evidence that climate change is affecting GLOF frequency. GLOFs are particularly common in the Baker River watershed (Patagonia, 47°S), where 21 GLOFs occurred between 2008 and 2017 due to the drainage of Cachet 2 Lake into the Colonia River, a tributary of the Baker River. During these GLOFs, the increased discharge from the Colonia River blocks the regular flow of the Baker River, resulting in the inundation of the Valle Grande floodplain, which is located approximately 4 km upstream of the confluence. To assess the possible relationship between GLOF frequency and climate variability, four sediment cores collected in the Valle Grande floodplain were analyzed. Their geophysical and sedimentological properties were examined, and radiocarbon-based age-depth models were constructed. All cores consist of dense, fine-grained, organic-poor material alternating with low-density organic-rich deposits. The percentage of lithogenic particles, which were most likely deposited during high-magnitude GLOFs, was used to reconstruct the flood history of the last 2.75 kyr. Results show increased flood activity between 2.57 and 2.17 cal kyr BP, and between 0.75 and 0 cal kyr BP. These two periods coincide with Neoglacial advances that are coeval with periods of lower temperature and increased precipitation. Our results suggest that GLOFs are not a new phenomenon in the region. Although rapid glacier retreat is likely responsible for high GLOF frequency in the 21st century, high-magnitude GLOFs seem to occur more frequently when glaciers are larger and thicker.

1. Introduction

Glacial Lake Outburst Floods (GLOFs) occur when a lake dammed by a glacier or moraine suddenly empties, resulting in the abrupt flooding of downstream environments (e.g., Benn and Evans, 2010). In glacierized regions, these events constitute a constant threat to infrastructure, livestock, and human lives. Historical data worldwide suggest that GLOFs have occurred throughout recorded history (Carrivick and Tweed, 2016). There is however only limited evidence that their frequency has changed (IPCC, 2019).

The recent increase of glacial lakes, both in size and number (e.g., Paul et al., 2007; Wang et al., 2011; Davies and Glasser, 2012; Carrivick and Quincey, 2014; Aniya, 2017; Prakash and Nagarajan, 2018; Wilson et al., 2018; Zhang et al., 2019), has led to the assumption that GLOF frequency is currently increasing, mostly due to increased glacier retreat and thinning rates (e.g., Iribarren Anacona et al., 2014; Wilson et al., 2018). However, recent studies suggest that the number of GLOFs has actually reduced since the mid-1990s in all major world regions (Carrivick and Tweed, 2016). A recent global inventory of GLOFs originating from the failure of moraine dams shows a global increase in flood frequency between 1930 and 1970, followed by a decline in recent decades, despite

* Corresponding author.
E-mail address: Elke.Vandekerkhove@UGent.be (E. Vandekerkhove).

https://doi.org/10.1016/j.quascirev.2020.106572

glacier recession (Harrison et al., 2018). The global increase in GLOF frequency around 1930 was associated with a delayed response to the warming that ended the Little Ice Age (LIA) and the recent decrease in GLOF frequency and regularity was interpreted as reflecting the climate stabilization that followed the LIA (Harrison et al., 2018). Carrivick and Tweed (2016), however, did not observe any significant trend in the number of GLOFs from moraine-dammed lakes over the last 50 years. By comparison, GLOFs from ice-dammed lakes are also known to occur during periods of glacier growth (Benn and Evans, 2010; Round et al., 2017), and their frequency globally seems to have decreased over the last 50 years (Carrivick and Tweed, 2016).

In Patagonia, GLOF frequency appears to have increased in the last three decades (Iribarren Anacona et al., 2014). They are particularly pronounced in the Baker River watershed (47–48°S), which drains most of the eastern side of the Northern Patagonian Icefield (NPI). The Colonia River, which is a tributary of the Baker River, experienced repeated GLOF events from 1881 onwards (Tanaka, 1980; Winchester and Harrison, 2000; Jacquet et al., 2017). After a 50-year long period of quiescence between the 1960s and 2008 during which no GLOFs were documented, GLOFs in the Baker River watershed restarted in April 2008, with a frequency of 1–3 per year (Jacquet et al., 2017). These GLOFs all initiated from the emptying of Cachet 2 Lake into the Colonia River (Dussaillant et al., 2010; Jacquet et al., 2017). During these events, the discharge of the Baker River roughly triples, resulting in the inundation of large floodplains.

This apparent abrupt increase in GLOF frequency in the Colonia River valley has reinvigorated discussions about the possible link between climate change and GLOF frequency. However, there is currently no conclusive answer to this question, mainly because of a lack of continuous flood records on timescales that extend beyond gauged river-flow datasets. Long-term flood records that allow for an evaluation of the drivers of flood frequency can be obtained from geological archives, such as floodplain sediments, which have proven to be valuable recorders of flood variability (e.g., Paine et al., 2002; Jones et al., 2012; Toonen et al., 2015; Lintern et al., 2016; Ishii et al., 2017; Fuller et al., 2018, 2019).

The aim of this paper is to reconstruct Baker River flood variability during the late Holocene to evaluate long-term (pre-instrumental) changes in GLOF frequency. We do so by analyzing geophysical and sedimentological data obtained on four independently-dated sediment cores collected in the Valle Grande floodplain, which is located along the upper Baker River. The results are then compared to proxy records of both glacier and climate variability to assess their potential relationships.

2. Setting

2.1. Hydrology

The Baker River (47–48°S) is located in Chilean Patagonia (Fig. 1a). It is the largest river in Chile in terms of mean annual discharge (~1100 m^3/sec; Dussaillant et al., 2012). The river originates from Bertrand Lake, which is directly fed by General Carrera Lake, and continues to flow southwards where it discharges into the Martínez Channel near the town of Tortel (Fig. 1a). Along its approximate 190 km course, the Baker River receives meltwater from NPI outlet glaciers via (from North to South) the Nef, Colonia, and Ventisquero rivers. It is also fed by the Chacabuco, Cochrane, Del Salto, and De Los Ñadis rivers, which originate from the eastern side of the watershed. The Del Salto and De Los Ñadis rivers both receive meltwater from small mountain glaciers on the eastern side of the Baker watershed. Due to the glacial regime of the Baker River, its discharge varies seasonally from 600 m^3/s in winter to 1200 m^3/s in summer (Dussaillant et al., 2012).

2.2. Glaciology

The NPI, with a surface area of approximately 4000 km^2 (Davies and Glasser, 2012; Aniya, 2017), is the second largest temperate icefield. After the Last Glacial Maximum, NPI glaciers contracted and expanded several times, and different chronologies of Neoglacial advances have been postulated for the Holocene (Mercer, 1982; Aniya, 1995, 1996, 2013; Davies et al., 2020). The chronology proposed by Aniya (2013) is one of the most detailed and it includes five Neoglaciations at 5.1–4.5 cal kyr BP, 4.0–3.6 cal kyr BP, 2.8–2.0 cal kyr BP, 1.6–0.9 cal kyr BP, and during the 17th–19th centuries. This chronology, however, is mostly based on data from outlet glaciers of the SPI (Southern Patagonian Icefield), as studies of Holocene NPI glacier variability remain very limited. The most recent review of Patagonian glacier evolution by Davies et al. (2020) only briefly addresses Neoglacial advances but it suggests that glaciers advanced or stabilized at 6–5 cal kyr BP, 2–1 cal kyr BP, and 0.5–0.2 cal kyr BP, although Nimick et al. (2016) observed a clear advance of the Colonia Glacier at 2.9 cal kyr BP, in agreement with the formation of a large moraine by glacier Leones slightly before 2.5 cal kyr BP (Harrison et al., 2008). After the latest advance in the 17th–19th centuries, which is frequently associated to the LIA, all eastern NPI glaciers receded (Masiokas et al., 2009). Their total surface area loss between 1870 and 2011 has been estimated at 19.1% (Davies and Glasser, 2012). Similarly, smaller mountain glaciers located to the East of the NPI and discharging into the Del Salto and De Los Ñadis rivers, have experienced a general ice retreat during the last ~150 years (Davies and Glasser, 2012).

2.3. Holocene GLOFs in the upper Baker River area

Very few paleohydrological reconstructions exist along the eastern side of the NPI, and most focus on the catastrophic floods that occurred during the deglaciation (e.g., Benito and Thorndycraft, 2020). The oldest evidence of GLOF occurrence in the upper Baker River area, as identified from erosive and depositional landforms, dates back to ~12.6–11.7 kyr BP (Benito and Thorndycraft, 2020). These megaflood-type landform assemblages resulted from catastrophic floods, with volumes of around 100 km^3, at a time when the discharge of large proglacial lakes was being reorganized towards the Pacific Ocean via the Baker River (Turner et al., 2005; Glasser et al., 2016; Thorndycraft et al., 2019). During the Holocene, additional paleofloods were identified from slackwater deposits found immediately downstream of the Baker-Colonia confluence (Benito et al., 2014; Benito and Thorndycraft, 2020). The latter deposits provide evidence for at least eight floods between 7.0 and 2.5 cal kyr BP and at least three GLOFs during the last 600 years, separated by a stable period between 2.5 and 0.6 cal kyr BP. Although Lara et al. (2015) used tree rings to reconstruct Baker River streamflow during the last 250 years, their record is unfortunately insensitive to GLOFs.

The first historical evidence of GLOF occurrence in the upper Baker River area dates back to the early 1880s (Tanaka, 1980). These GLOFs originated from the Colonia River and are related to the retreat of Colonia Glacier between 1850 and 1880 (Harrison and Winchester, 2000). Due to this retreat, Arco Lake, which was at the time dammed by Colonia Glacier, released approximately 265×10^6 m^3 of water around 1881 (Tanaka, 1980; Winchester and Harrison, 2000, Fig. 1a). Afterwards, repeated GLOFs occurred in the Colonia valley from water discharged by Arco Lake. Severe flood events took place c. 1896/1897, 1914/1917, 1944 and 1963, until a drainage path eventually established between Arco and Colonia lakes in the 1960s and GLOFs ceased to occur (Winchester and

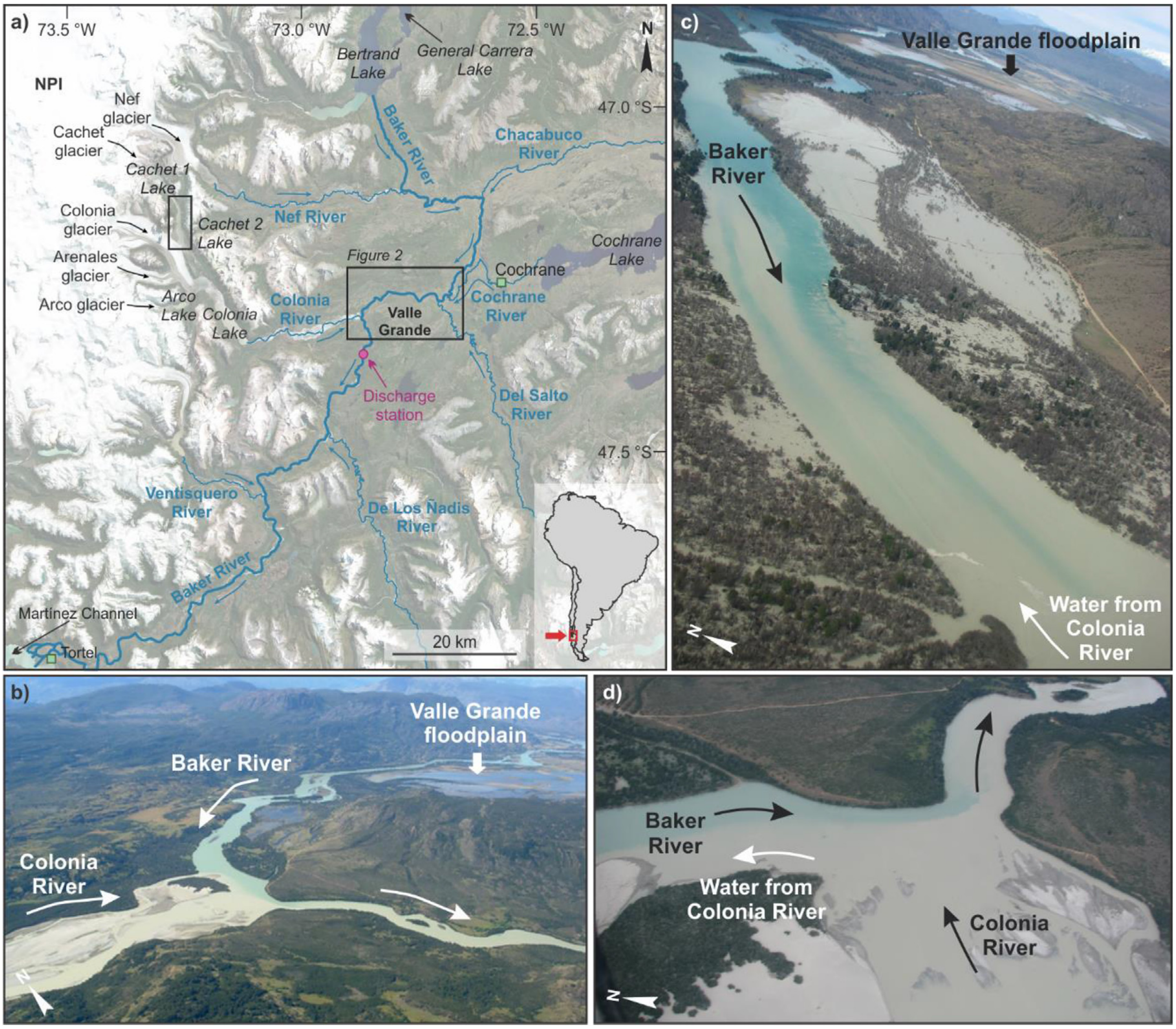

Fig. 1. Location of the Valle Grande floodplain along the Baker River in Chilean Patagonia. (a) Location of the Baker River in its entire course from Bertrand Lake to Martinez Channel, with indication of the main tributaries and glaciers discussed in the text (Global Mapper World Imagery). NPI stands for Northern Patagonian Icefield. The towns of Cochrane and Tortel are indicated with green squares. (b) Location of Valle Grande, four km upstream of the confluence between Baker and Colonia rivers. This image was taken in February 2009, during the only known inundation of the Valle Grande floodplain due to heavy rainfall (photo credit: Horacio Parrague). (c) Sediment from the Colonia River flowing upstream in the Baker River towards Valle Grande during the September 2016 GLOF. This GLOF resulted in the partial inundation of the Valle Grande floodplain due to backwater flooding (photo credit: Andrés Rivera). (d) Confluence of Colonia and Baker rivers during the December 2008 GLOF where water and sediment are flowing upstream (towards the north) in the Baker River (photo credit: Paulina Rojas). Note the lack of sediment flowing upstream during the precipitation-driven flood in (b). (For interpretation of the references to color in this figure legend, the reader is referred to the Web version of this article.)

Harrison, 2000; Jacquet et al., 2017).

The Colonia River experienced a new series of repeated GLOFs between April 2008 and November 2017 (Dussaillant et al., 2010; Jacquet et al., 2017). These events all resulted from the abrupt drainage of Cachet 2 Lake into the Colonia River, generally through a subglacial tunnel below the Colonia Glacier (Fig. 1a; Dussaillant et al., 2010; Friesen et al., 2015). During such a GLOF event, the Baker River downstream of the confluence with the Colonia River can triple in discharge, reaching between 3000 and 3800 m^3/sec (Dussaillant et al., 2010). A total of 21 GLOFs have been recorded since April 2008 (Jacquet et al., 2017; DGA, Chile). Photographic and conversational evidence indicate that most Colonia River GLOFs result in the inundation of the Valle Grande floodplain, which is located immediately upstream of the confluence with the Colonia River (Fig. 1b and c and Supplementary Fig. S1). This flooding results from the blocking of the regular Baker River water flow towards the South by the Colonia River, which in turn results in Baker River water levels rising by 4–6 m (Supplementary Table S1; Oportus, 1928).

Historical documents suggest that the Nef River, which discharges into the Baker River upstream of Valle Grande (Fig. 1a), also experienced GLOFs during the last century (Supplementary Table S1; Oportus, 1928; De Agostini, 1945). These events similarly resulted in the flooding of Valle Grande. However, the GLOFs originating from the Nef valley in the 1940s were of lower magnitude compared to those from the Colonia valley, and they only resulted in a partial inundation of the floodplain (De Agostini, 1945). The other rivers that discharge into the Baker River near Valle Grande (Chacabuco, Cochrane, and Del Salto rivers; Fig. 1a) have no historical records of GLOFs.

2.4. Valle Grande floodplain

The Valle Grande floodplain (47.30 °S; 72.75 °W) is located

10 km to the west of the town of Cochrane, in the upper reaches of the Baker River, approximately 4 km upstream of its confluence with the Colonia River (Figs. 1a and 2a). It has a surface area of 50 km^2 and it is the largest area of Holocene alluvial sediments along the Baker River (Ulloa et al., 2018; Benito and Thorndycraft, 2020). The sinuous Baker River meanders through the northern part of this flat area for almost 15 km and the Del Salto River crosses its eastern end before flowing into the Baker River. The floodplain, which is considerably wider south of the Baker River, contains many paleochannels and a few scroll bars (Fig. 2a). The paleochannels are defined by vegetated and sinuous ridges, which represent old river levees (Fig. 2b). Similarly, scroll bars occur as curved elevated ridges in the floodplain. The floodplain morphology is interpreted to be shaped by Holocene floods, including GLOFs from Nef and Colonia valleys (Benito and Thorndycraft, 2020). On the right bank of the Baker River, the floodplain is rather narrow and consists mainly of marshland with a few small ponds and patches of dense forest (Fig. 2a). On the left bank, grasslands and marshland dominate the lower elevated regions. Remaining patches of *Nothofagus* forest and scrub occur on the slightly elevated areas. Here, the floodplain is primarily used as pastureland, for which most of the original forest was cleared by

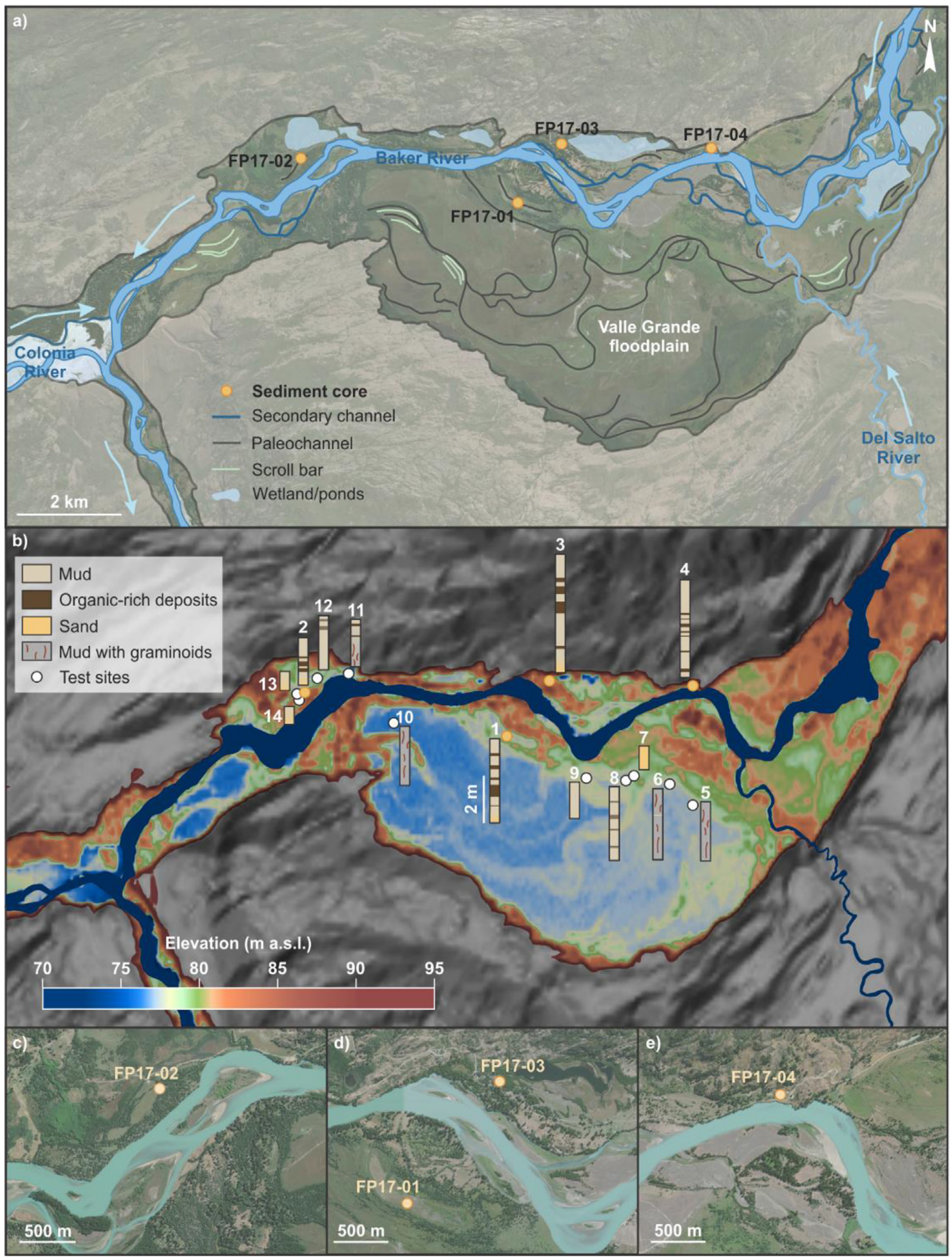

Fig. 2. Location of the sediment cores collected in the Valle Grande floodplain. (a) Google Earth Imagery with the location of the four sediment cores used in this study. (b) TanDEM-X elevation map of the Valle Grande floodplain (Wessel et al., 2018; color scale for elevations <95 m a.s.l.). The grey-level background (elevations >95 m a.s.l.) is from SRTM. Simplified lithologs based on field core descriptions are displayed for the four cores (orange dots) as well as for the test locations (white dots). The absolute elevations (a.s.l.) of the collected sediment cores are 76.9 m, 80.2 m, 81.0 m, and 79.0 m for FP17-01, FP17-02, FP17-03, and FP17-04, respectively (vertical mean error <0.2 m; Wessel et al., 2018). The average Baker River elevation along the floodplain is approximately 75.0 m, with a slope of 0.01° (~2m/10 km). The coring locations are enlarged in (c), (d), and (e). (For interpretation of the references to color in this figure legend, the reader is referred to the Web version of this article.)

burning during the first half of the 20th century (De Agostini, 1945).

In addition to GLOFs, the Valle Grande floodplain can also flood during long-lasting (several days) extreme precipitation events. Such an event occurred in February 2009, during which the Baker River discharge increased to 2700 m^3/sec and the Baker river water level increased by 2.5 m downstream of the confluence with the Colonia River, in response to five consecutive days of heavy rainfall (DGA, Chile; Fig. 1a and b and Supplementary Fig. S1). The February 2009 event is the only rainfall-induced flooding event reported in regional archives. By comparison, water level during the 21st century Cachet 2 GLOFs rose by an additional ~1 m (DGA, Chile).

2.5. Present-day climate

Precipitation patterns in Patagonia (>40°S) display a strong longitudinal gradient driven by the blocking of humid air masses from the Pacific Ocean by the Andes. A hyperhumid climate prevails on the western side of the Andes where mean annual precipitation ranges from 5000 to 10 000 mm (Garreaud et al., 2013). There, the amount of precipitation is directly related to the strength of the Southern Westerly Wind Belt (SWWB). In eastern Patagonia, on the other hand, forced subsidence causes precipitation to decrease rapidly to less than 300 mm/yr, resulting in an arid climate (Garreaud et al., 2013). Valle Grande, which is located immediately to the east of the NPI, exhibits annual precipitation amounts of 695 mm/yr (Lenaerts et al., 2014), 934 mm/yr (WorldClim v. 2.1; Fick and Hijmans, 2017) or 933 mm/yr (CR2MET; Alvarez-Garreton, 2018) based on gridded climate data. In general, this region experiences wetter conditions in austral winter (305 mm) compared to austral summer (168 mm; WorldClim v. 2.1). The seasonal temperature difference is about 10 °C, with mean winter and summer temperatures of 4.1 °C and 14.0 °C, respectively (WorldClim v. 2.1).

3. Materials and methods

3.1. Sampling

Valle Grande was selected after an exploratory survey along the Baker River. Based on our observations, this floodplain seems to be the only one preserving a continuous flood stratigraphy. In addition, Valle Grande is located downstream of several glacial valleys. Its sediment record therefore integrates floods originating from several glacier-river systems, making it relatively independent of the evolution of any specific proglacial lake. Coring locations were selected based on their relative elevation above the Baker River, i.e., less than 6 m difference, as this corresponds to the water level rise of the Baker River during the largest historical GLOFs (Supplementary Table S1). In summer 2016, a 25 mm diameter gouge auger was used to test 14 sites on both sides of the river, from which complete lithological descriptions were made (Fig. 2b). Four sites containing a complete and undisturbed stratigraphy were selected for sampling with a 52 mm diameter Russian corer in January 2017: three to the north of the river and one to the south (Fig. 2b–e). The sediment cores were collected in 50 cm-long sections from two different holes with a 25 cm overlap to obtain a continuous composite core at each site. All sections were stored in PVC liners and wrapped in plastic foil. The upper 50 cm was sampled using 23 cm-long aluminum boxes (4 × 4 cm) and were, as for the 50-cm long sections, collected at overlapping depth intervals and wrapped in plastic foil.

3.2. Sedimentological and geophysical analysis

All the Russian sediment core sections were described, imaged (linescan) and logged with a Geotek Multi-Sensor Core Logger (MSCL) at Ghent University (Belgium). Logging of gamma-ray density (^{137}Cs source) was performed at a 2 mm interval. Composite cores were made based on core descriptions and Geotek MSCL data. Afterwards, the composite cores were subsampled at a 5 mm interval, and samples were weighed, freeze-dried, and weighed again to determine their water content.

Loss-on-Ignition (LOI) was measured continuously at 5 mm resolution following Heiri et al. (2001). After freeze drying the samples, approximately 0.25 g of sediment was oven dried overnight at 105 °C and then heated at 550 °C for 4 h. The weight loss after combustion at 550 °C was used to estimate the organic content, i.e., LOI550. The inorganic content was determined by difference (100% - LOI550). Five duplicate analyses on three different samples indicated a relative error of 2.82% (1σ). The amount of carbonate was not quantified since test measurements showed that it was negligible (LOI1000: 0.7 ± 0.5%; n = 72), in agreement with the regional lithology (Sernageomin, 2003).

Grain-size measurements were conducted on core FP17-01 at 2 cm resolution using a Malvern Mastersizer 3000 equipped with a Hydro MV dispersion module at Ghent University (Belgium). Resolution was increased to 1 cm between 0–25 cm and 44–97 cm, and to 5 mm between 26–43 cm and 98–124 cm, to capture the fine laminations described in the upper part of the core. Samples with LOI550 values >5% were first heated at 550 °C for 4 h to remove organic matter. All samples were pre-treated by adding a 30% hydrogen peroxide (H_2O_2) solution to 10 ml of de-ionized water containing the suspended sediment and set to boil until the reaction ended. Afterwards, 1 ml of HCl (10%) was added to the samples to remove carbonates. After rinsing, biogenic silica was removed by adding 1 ml of NaOH (2N). Finally, all samples were decanted before sodium hexametaphosphate was added to avoid grain flocculation. Samples were measured in triplicates during 12 s with 10% sonification.

3.3. Core chronologies

Radiocarbon ages, charcoal counts, and ^{210}Pb activities were obtained to establish core chronologies. Samples for radiocarbon analysis were selected in organic-rich deposits near sharp lithological boundaries (Fig. 3) and examined to identify macrofossils. All samples were pretreated following established protocols (Mauquoy et al., 2004). The selection of monospecific plant macrofossils for radiocarbon analysis minimized the risk of age contamination (by, e.g., plant roots). Measurements were made with an accelerator mass spectrometer at DirectAMS (USA). In addition, one bulk sediment sample from the bottom of core FP17-01 was oven dried and analyzed at NOSAMS (USA).

Age-depth models were constructed independently for each core using two to six radiocarbon ages per core (Table 1). All ages were calibrated using the latest calibration curve for the Southern Hemisphere (SHCal13; Hogg et al., 2013). The 'proxy-ghost' function of BACON 2.3.6 was used to visualize chronological uncertainties (Blaauw and Christen, 2011).

In order to refine core chronologies at the top of the cores, charcoal was counted at 1 cm resolution in the upper 140 cm and 130 cm of FP17-01 and FP17-03, respectively, at the Montana State University Paleoecology Laboratory (USA). In addition, ^{210}Pb measurements were conducted using alpha spectrometry at a 10 cm interval down to 60 and 70 cm on FP17-01 and FP17-03, respectively, at the Australian Nuclear Science and Technology Organisation (ANSTO, Australia), following methods described in Harrison et al. (2003).

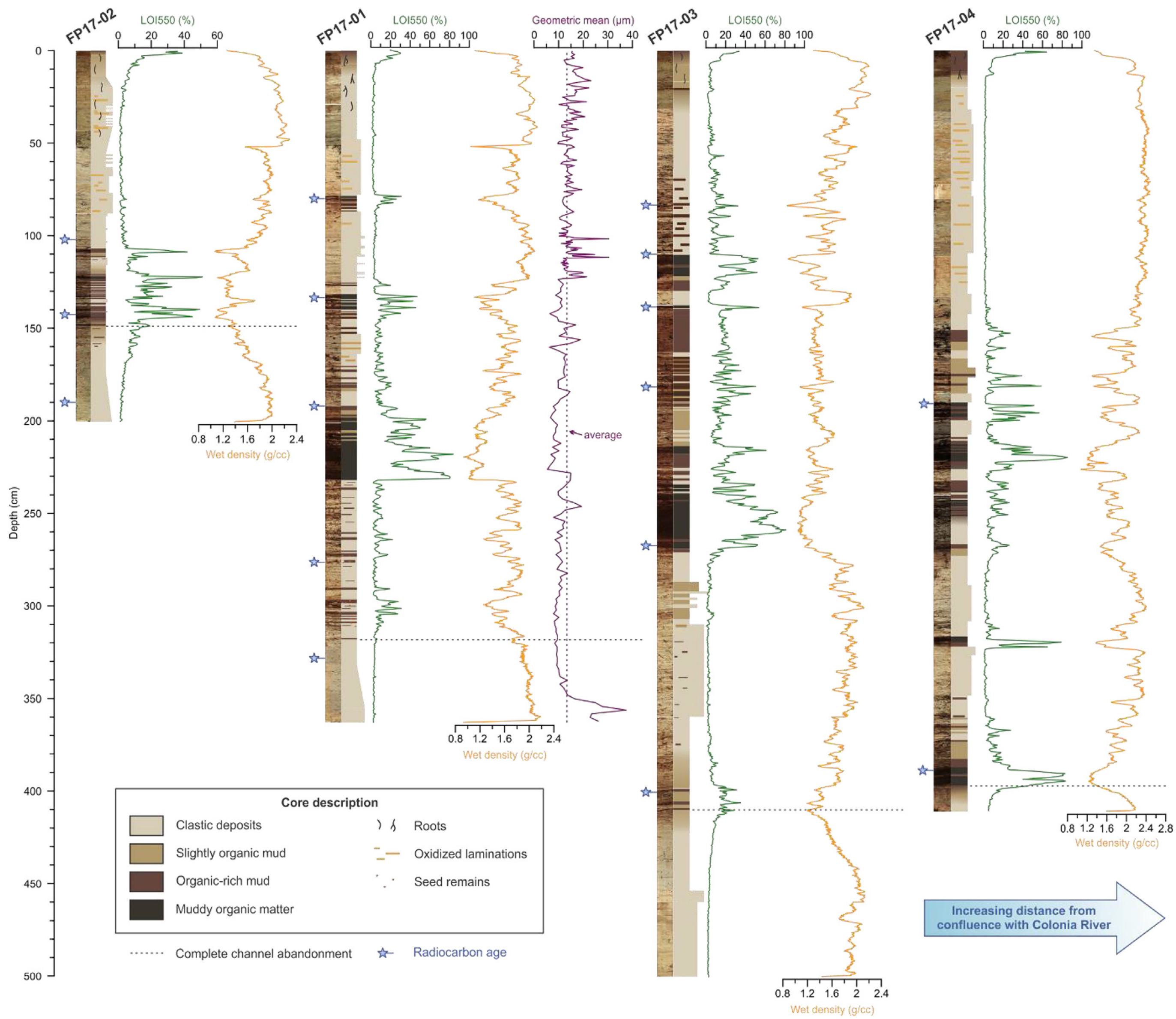

Fig. 3. Lithology of composite sediment cores FP17-02, FP17-01, FP17-03, and FP17-04, i.e., organized with increasing distance from the confluence with the Colonia River (see Fig. 2a). Photographs are on the left, next to the lithologs. For all cores, LOI550 and wet density are displayed. For FP17-01, the geometric grain-size mean and its average value for the core (dashed purple line) are also shown. Horizontal dashed black lines represent the start of the occurrence of autochthonous sedimentation and are defined at depths of 149, 318, 411, and 397 cm for FP17-02, FP17-01, FP17-03, and FP17-04, respectively. (For interpretation of the references to color in this figure legend, the reader is referred to the Web version of this article.)

3.4. Suspended sediment concentrations

The rivers discharging into the Baker River upstream (Nef, Chacabuco, Cochrane, Del Salto) and immediately downstream (Colonia) of Valle Grande (Fig. 1) were sampled for Suspended Sediment Concentration (SSC) measurement. Three sites were also sampled along the Baker River. These rivers were sampled throughout the year (n per river = 8–21) between 2008 and 2010. SSC values were obtained after manual filtration on GFF filters until saturation. Annual sediment yields were calculated by multiplying SSC by the annual volumes of water (from Dussaillant et al., 2012).

4. Results

4.1. Lithology

The sediments of all test sites, except for location 7, are dominated by mud, with frequent intercalations of organic-rich deposits (Fig. 2b). Sediments from the lower elevations consist mainly of mud with reddish graminoid remains, whereas higher locations are composed of mud alternating with organic-rich deposits. Some of the sites display a coarse sand base, and a single location, i.e., test site 7, is fully composed of sand.

In the four Russian sediment cores, which are all located at higher elevations (Fig. 2), four major facies can be identified: clastic deposits, slightly organic mud, organic-rich mud, and muddy organic matter (Fig. 3). The clastic deposits are composed of dense

Table 1
Radiocarbon ages obtained on sediment cores FP17-01 to FP17-04. The ages were calibrated with Clam 2.3.4 (Blaauw, 2010), using the SHCal13 calibration curve (Hogg et al., 2013).

Core label, location, and sample depth (cm)	Dated material	$\delta^{13}C$	^{14}C age (yrs BP ± 1σ)	2σ calibrated age range (cal yr BP)	Laboratory code
FP17–01 (47.28°S–72.77°W)					
80.0–80.5	Carex spp. leaf bases	−27.2	748 ± 26	568–682	D-AMS 028297
133.5–134.0	Carex spp. leaf bases	−30.0	1287 ± 30	1072–1267	D-AMS 031344
192.0–192.5	Carex spp. leaf bases	−28.7	1367 ± 27	1185–1297	D-AMS 028298
276.5–277.0	Carex spp. leaf bases	−28.8	2076 ± 30	1922–2084	D-AMS 028299
328.5–329.0	Bulk organic matter	−25.5	2320 ± 20	2183–2351	OS-135980
FP17–02 (47.27°S–72.82°W)					
102.0–102.5	Carex spp. leaf bases	−29.5	1050 ± 20	819–959	D-AMS 028300
142.5–143.0	Carex spp. leaf bases	−28.2	1227 ± 29	986–1181	D-AMS 028301
190.0–190.5	Carex spp. leaf bases	−26.4	1498 ± 23	1303–1374	D-AMS 028302
FP17–03 (47.27°S–72.76°W)					
83.5–84.0	Carex spp. leaf bases	−23.5	438 ± 25	334–506	D-AMS 028303
110.0–110.5	Carex spp. leaf bases	−22.9	607 ± 23	529–629	D-AMS 028304
138.5–139.0	Carex spp. leaf bases	−23.5	788 ± 26	658–724	D-AMS 028305
181.5–182.0	Carex spp. leaf bases	−16.3	1693 ± 27	1435–1692	D-AMS 028306
267.5–268.0	Carex spp. leaf bases	−28.1	2225 ± 32	2096–2313	D-AMS 031345
400.5–401.0	Carex spp. leaf bases	−29.5	2572 ± 32	2489–2747	D-AMS 031346
FP17–04 (47.27°S–72.72°W)					
191.0–191.5	Carex spp. leaf bases	−25.1	1133 ± 22	935–1057	D-AMS 028307
389.0–389.5	Carex spp. leaf bases	−32.1	2594 ± 34	2491–2755	D-AMS 031347

inorganic material with little or no organic matter (LOI550 <10%). Slightly organic mud and organic-rich mud represent a mixture of mud and organic matter with variable density and LOI550 values. The muddy organic matter deposits are generally thick, have LOI550 values exceeding 65%, and density values <1.4 g/cc (Fig. 3).

The upper part of all four cores is composed of clastic sediments (Fig. 3). The uppermost 10–20 cm, however, consists of modern soil, with LOI550 values increasing from bottom to top in the upper 10 cm. Root remains are visible down to a depth of 50 cm (Fig. 3). Discoloration by oxidation is abundant in the upper 45 cm and between 65 and 90 cm depth in FP17-02, and in the upper 130 cm in FP17-04. Three of the four cores, i.e., FP17-02, FP17-01, and FP17-03, display a fining upward trend at the bottom, from coarse sand towards silt. Grain-size measurements confirm this fining upward trend at the bottom of core FP17-01 (Fig. 3). These grain-size measurements also show that FP17-01 sediments mainly correspond to unimodal silts with a mean grain size of 13.4 ± 4.2 μm (1σ; Supplementary Fig. S2). The sediments are slightly coarser towards the top of the core. Coarser cm-thick silt layers can be found at a depth of 100–123 cm in FP17-01, where mean grain size reaches up to 30 μm. Muddy organic matter deposits can be found in FP17-01 and FP17-03 between 200 and 230 cm, and 230 and 270 cm, respectively. In FP17-04, muddy organic matter deposits occur from 190 to 200 cm, 210–215 cm, 230–250 cm, and 380–400 cm. In FP17-02, two one-cm thick layers of muddy organic matter are found at 123 and 140 cm.

4.2. Age-depth models

^{210}Pb could not be used to establish core chronologies as unsupported ^{210}Pb activities were not detected in most of the samples below the surface (Supplementary Tables S2 and S3). This suggests that the upper 10 cm of the sediment cores represent more than 150 years of sedimentation, which is supported by the relatively high organic content of these samples (Fig. 2), indicative of a period of slow sediment accumulation that promoted soil development. Likewise, charcoal concentrations are strongly related to organic matter content and likely represent pre-historical fire events, and thus could not be used to develop core chronologies by comparison with historical fire occurrences (Supplementary Fig. S3). The age-depth models were therefore entirely based on radiocarbon ages (Fig. 4). They reveal that the bottom of FP17-01, FP17-02, FP17-03, and FP17-04 reach ages of 2690 ± 251, 1465 ± 133, 3176 ± 235, and 2890 ± 225 cal yr BP, respectively (Fig. 4). The average sedimentation rates of the four cores are very consistent and vary between 0.13 and 0.16 cm/yr.

4.3. Suspended sediment concentrations

The Baker River near its source has very low SSC (1.4 ± 1.0 mg/L; Fig. 5, Supplementary Table S4). On its way to the Valle Grande floodplain, it picks up sediment from rivers Nef (65 ± 20 mg/L), Chacabuco (88 ± 148 mg/L), Cochrane (3.1 ± 1.3 mg/L) and Del Salto (17 ± 16 mg/L). By comparison to these rivers, SSC values in the proglacial Colonia River are significantly higher (226 ± 117 mg/L). Although SSC values during GLOFs are unknown in the Valle Grande area, extreme values of 579 mg/L and 435 mg/L were measured in rivers Chacabuco and Baker after intense precipitation, which is similar to the regular summer values measured in the Colonia River (212–525 mg/L). In terms of sediment yield, the Colonia River also displays the highest values (0.99 × 10^6 T/yr), which is more than double the yield of the Baker River immediately upstream of its confluence with the Colonia River (0.45 × 10^6 T/yr; Fig. 5).

5. Discussion

5.1. Sedimentological interpretation

The sedimentary infill of all investigated locations in the Valle Grande floodplain varies with location (Fig. 2b). In general, floodplain elevation appears to play an important role in determining the nature of the sedimentary infill. Sites at lower elevation (<76 m a.s.l., i.e., within 1m of the regular Baker River level) display a continuous clastic infill (mud or mud with graminoids) and are therefore not suited for flood reconstruction, whereas those above 76 m a.s.l. display flood deposits (mud) intercalated within autochthonous sediments (peat or gyttja). Sites at higher elevation are less frequently flooded, which allows autochthonous sedimentation to occur. These locations could thus provide accurate archives of Baker River floods.

The four Russian sediment cores are all located at elevations above 76 m a.s.l. and show such alternations of clastic material and organic-rich sediments (Fig. 3). As such, they register periods when

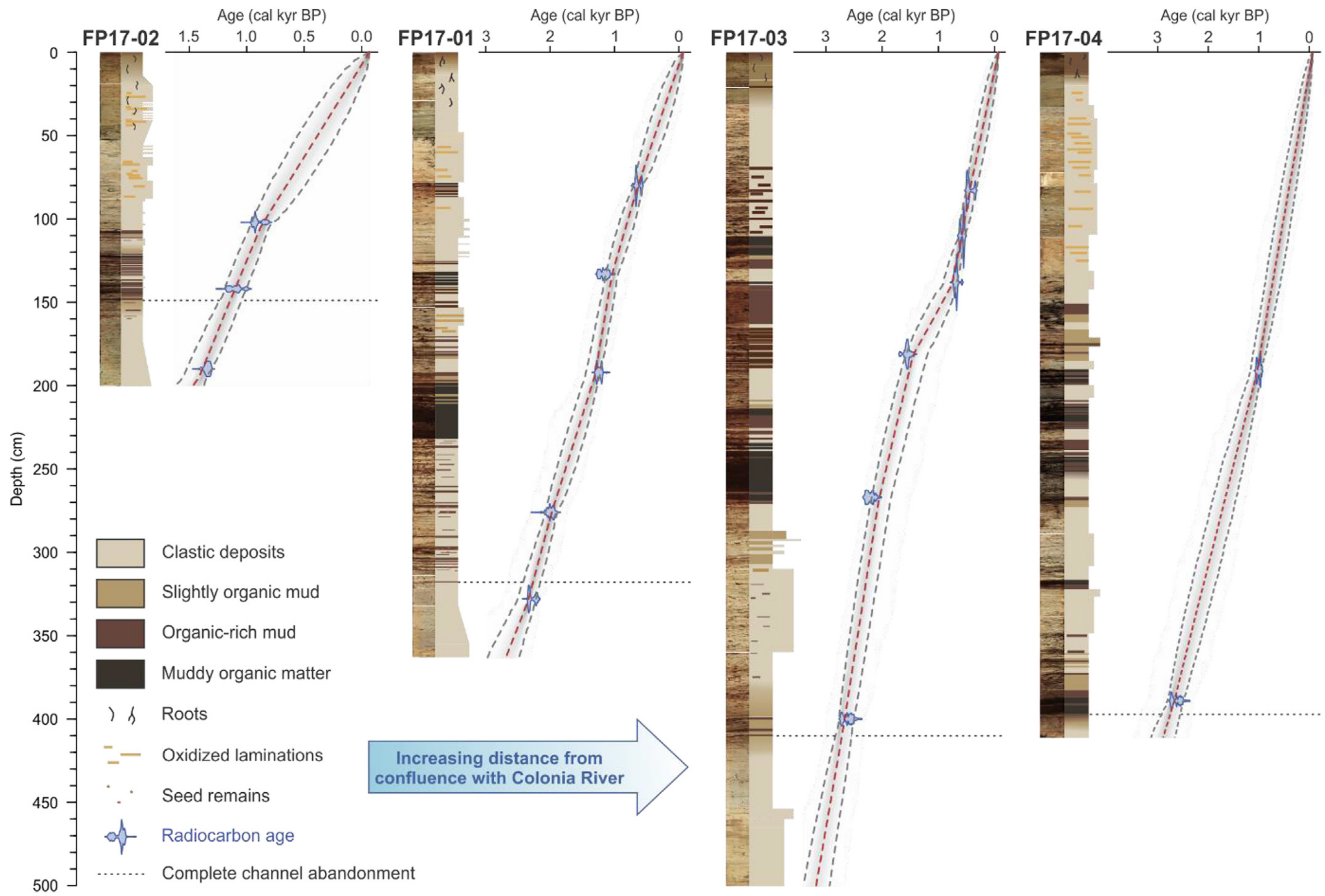

Fig. 4. Age-depth models and corresponding error envelopes constructed with BACON 2.3.6 (Blaauw and Christen, 2011) for the four sediment cores. The cores are organized by increasing distance from the confluence with the Colonia River.

flooding was frequent but they do not reveal individual flood layers. Therefore, they allow the reconstruction of periods of increased flood frequency, but they are not suitable to derive quantitative estimates of flood magnitude.

It should also be noted that the sensitivity of the coring sites to flooding most likely decreases through time due to sediment accretion. As sediment deposition progressively increases floodplain elevation, they will less frequently inundate with sediment-laden water (Nanson and Beach, 1977; Hooke, 1995; Saint-Laurent et al., 2010). River erosion also increases the elevation difference between the floodplain and river, resulting in a decrease in the sensitivity of the floodplain to high-magnitude floods through time.

The base of cores FP17-01, FP17-02, and FP17-03 is composed of fining-upward silts and sands (Fig. 3), which indicates a channel abandonment process (Hooke, 1995; Toonen et al., 2012; Dieras et al., 2013). At the very bottom of the cores, coarse sand was most likely deposited during the initial abandonment of the channel, when rapid infill by coarse river bedload occurs. The overlying fining-upward deposits represent the channel being progressively cut off from the main active channel, which resulted in the deposition of a finer suspended load consisting of mud, due to the gradually decreasing flow velocities within the channel (Toonen et al., 2012). This lithological transition from coarse sand towards a finer silt fraction is absent in FP17-04 as the bottom of the channel infill was most likely not reached during coring (Fig. 3).

The deposits above these channel silts and sands are composed of (a) clastic alluvial material alternating with (b) organic-rich deposits containing variable amounts of autochthonous organic matter (Fig. 3). These alternations are interpreted as flood (clastic) deposits intercalated in-between marsh-type (organic-rich) sediments that accumulate during periods of quiescence. Such laminated channel-fill sequences represent intermittent phases of flooding from the Baker River and indicate that a paleochannel reached the stage of disconnection (Toonen et al., 2012). When clastic sediment input is reduced during periods of quiescence, organic-rich (high LOI550) material can accumulate (Fig. 3). On the other hand, dense, organic-poor (low LOI550) sedimentation prevails during periods of flooding. The oxidized laminations in these sediments are most likely the result of redox reactions due to fluctuations in the water table (Fig. 3).

5.2. Flood reconstruction

Changes in sedimentology, more particularly fluctuations in the delivery of clastic material from the Baker River, are reflected by changes in LOI550 values. The input of inorganic alluvial material during flooding results in a decrease in the relative amount of organic matter, i.e., in LOI550. Consequently, the amount of inorganic material (100%−LOI550) presents a proxy for flood occurrence (e.g., Ishii et al., 2017). A flood reconstruction for each sediment core is inferred from the variations in inorganic material, which allows an evaluation of flood occurrence through time (Fig. 6a–d). For all cores, the start of the flood record is defined at

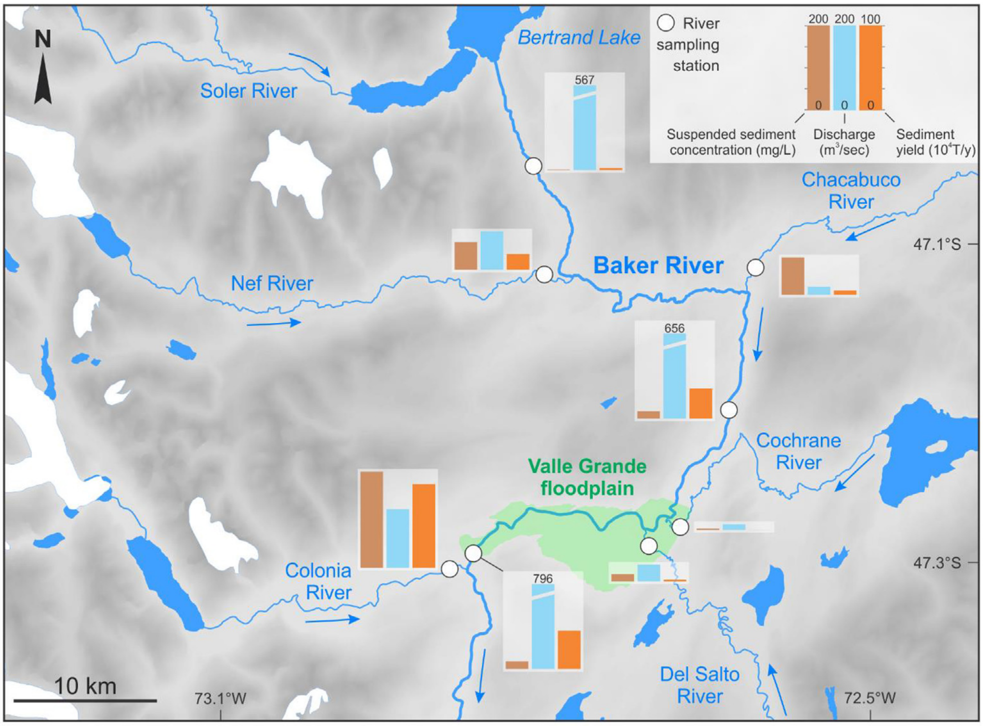

Fig. 5. Suspended sediment concentrations (SSC), river discharge and sediment yield in the Baker River tributaries around Valle Grande and along the Baker River itself. The SSC (n per site = 8–21) and river discharge (from Dussaillant et al., 2012) values are annual averages. The values are presented in appendix (Supplementary Table S4).

the onset of the laminated channel-fill sequence, where organic-rich sedimentation starts to occur after disconnection from the Baker River is completed (Fig. 3). For FP17-02, FP17-01, FP17-03, and FP17-04, the onset of the flood record corresponds to 1.14 ± 0.10 cal kyr BP, 2.27 ± 0.14 cal kyr BP, 2.72 ± 0.14 cal kyr BP, and 2.75 ± 0.18 cal kyr BP, respectively (Fig. 4).

To account for local variations in the sediment infill, including possible hiatuses, an average of the inorganic content of the four cores was established (Fig. 6e). The composite record, which dates back to 2.75 cal kyr BP, uses the age-depth models independently established for each core and is not based on lithological correlations. Two categories of flooding frequency can be defined in the composite record: high flood frequency (inorganic content >90%) and low flood frequency (inorganic content <90%). The results (Fig. 6e) reveal that flooding occurred throughout the past 2.75 cal kyr BP. However, two phases of high flood frequency occur between 2.57 and 2.17 cal kyr BP and between 0.75 and 0 cal kyr BP. Except for isolated peaks in LOI550 in FP17-01 and FP17-03 around 0.62 cal kyr BP, these two periods of increased flooding appear in all records. Two main periods of low flood frequency are present: a first one between c. 2.75 and 2.57 cal kyr BP, and a second between c. 2.17 and 0.75 cal kyr BP. It should be noted that both FP17-01 and FP17-04 show high flood activity between 2.17 and 1.70 cal kyr BP, whereas this time window is marked by high LOI550 values, and thus low flood activity, in FP17-03. Likewise, the most recent period of high flood frequency seems to start later in FP17-03 than in the other sediment cores, suggesting a lower sensitivity of this specific site, in agreement with its particularly high elevation (+6 m above the regular Baker River level). Despite apparent short increases in flooding around 1.80 and 1.15 cal kyr BP, the intermediate low flood frequency period between 2.17 and 0.75 cal kyr BP is consistent throughout all records. This period corresponds to the period identified as stable (dated at 2.5–0.6 cal kyr BP) in the stratigraphic record of Benito et al. (2014) below the confluence with the Colonia River.

5.3. *Origin of the floods recorded in Valle Grande sediments*

The input of inorganic material to the Valle Grande floodplain predominantly occurs by overbank flooding from the Baker River. The southern part of the floodplain could also be inundated by floods from the Del Salto River, but these would only be recorded in FP17-01, and possibly FP17-04 (Fig. 2). Historical information shows that both GLOFs and extreme precipitation floods can result in the inundation of Valle Grande. However, these two types of events may not leave the same signature in the sediment record.

Suspended sediment concentrations, and therefore the ability of the Valle Grande floodplain to record paleofloods, highly differ between GLOFs and precipitation-driven floods. Because the floodplain is located along the upper reaches of the Baker River, i.e., upstream of the confluence with most proglacial rivers (Fig. 1a), Baker River suspended sediment concentrations along the floodplain are generally very low (17 ± 17 mg/L; n = 18; Fig. 5). SSC at the outflow of the Colonia River, on the other hand, are much higher, i.e., 226 ± 117 mg/L (Fig. 5). Although SSC in other regional non-glacial rivers, such as Chacabuco, are not negligible, these rivers have a relatively low discharge year-round, resulting in low sediment yields (Fig. 5). Floods occurring during intense precipitation events might thus not supply sufficiently large amounts of clastic sediment to the floodplain to be registered as clear flood deposits, especially when compared to GLOFs, which are rich in suspended sediment of glacial origin. This is supported by observations made during some of the 21st century Cachet 2 GLOFs, during which SSC in the Baker River increased 8-fold downstream of the Colonia River confluence (Quiroga et al., 2011; Bastianon et al., 2012).

Historical information (Supplementary Table S1) and recent aerial photographs (Fig. 1c and d) describe that the flow of the Baker River reverses during Colonia River GLOFs over a distance of

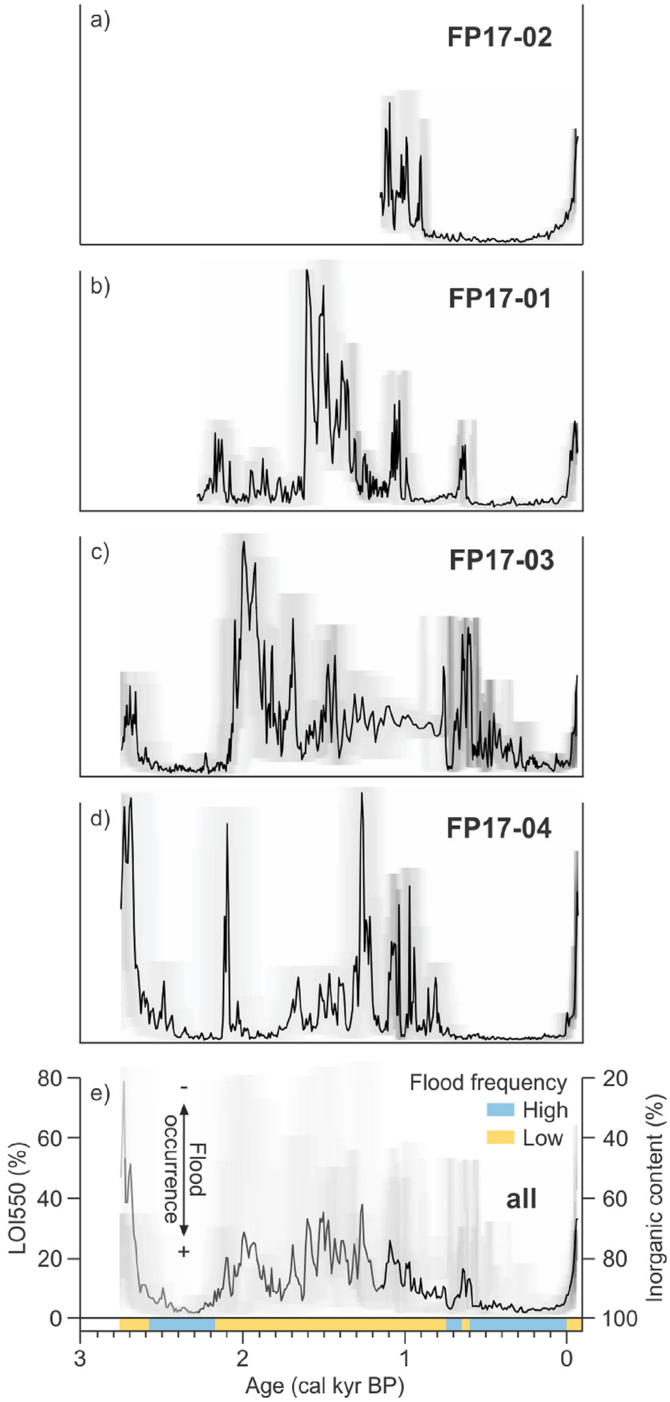

Fig. 6. LOI550 and inorganic content (100%–LOI550) versus time for the four floodplain sediment cores (a–d), plotted using the 'proxy-ghost' function of BACON 2.3.6 to visualize chronological uncertainties (Blaauw and Christen, 2011). Darker grey indicates higher probability. The lowermost graph (e) displays a composite curve based on the four records presented above. The grey level intensity of the solid line in the lowermost graph, represents the number of cores used to build the composite, darker corresponding to more cores.

up to 15 km upstream of the confluence with the Colonia River, thereby supplying glacial material from the Colonia River to the Valle Grande floodplain. In addition, GLOFs are the only events that are able to inundate the entire floodplain (De Agostini, 1945). Precipitation-driven floods only inundate the lower elevation areas (Fig. 1b). GLOFs also appear to occur more frequently than precipitation-driven floods in this glacierized region, as suggested by the high amount of GLOFs (21) versus precipitation-driven floods (1) that affected Valle Grande between 2008 and 2019, and they result in consistently higher (~1 m higher) Baker River levels immediately downstream of the confluence with the Colonia River.

Most of the sediment cores from Valle Grande contain cm-thick coarse silt layers at variable depth intervals (100–123 cm in FP17-01, 30–40 cm and 56–61 cm in FP17-02, and between 290 and 300 cm in FP17-03; Fig. 3). These deposits could result from higher magnitude floods, such as those originating upstream of the floodplain (e.g., from the Nef or Chacabuco rivers), as higher magnitude floods generally carry coarser particles. However, these layers could also represent meandering of the Baker River channel. Migration of the active river towards a coring site, or any change in the configuration of the floodplain that affects the connectivity between the river and a coring location (e.g., erosion of alluvial ridges that act as barriers for alluvial sediment transport), could increase the sensitivity of a site to floods. Eventually, this could cause a sudden increase in clastic input (e.g., Minderhoud et al., 2016) or the deposition of coarser sediments (e.g., Toonen et al., 2015) at one specific site. The absence of sand layers in core FP17-04 and the asynchronicity of these clastic layers in the three other cores favor this hypothesis. The influence, however, of any spatial variations in sediment deposition within the floodplain is minimized by reconstructing the flood history from the composite record, which is based on four different coring sites.

The consistently unimodal grain-size distributions throughout core FP17-01 (Supplementary Fig. S2) suggest that the clastic sediments represent one dominant depositional process (Fig. 3). Although the relatively low mean grain size throughout core FP17-01 (10–15 μm; Fig. 3) is compatible with a glacial origin of the sediment, it could also reflect non-glacial overbank flooding. The FP17-01 grain-size record also reveals a slight coarsening upward, which is particularly marked in the upper ~50 cm (~400 years) of the core. This suggests increased connectivity with the active river channel, although the nearest meander appears to be moving away from site FP17-01 (Fig. 2). Another explanation is that this increase in grain size during the last 400 years represents higher magnitude floods. This is supported by the identification of at least three GLOF deposits younger than 0.6 kyr BP in the stratigraphic record of Benito et al. (2014), which is located immediately downstream of the Colonia-Baker confluence. Since the latter site has a much higher flood sensitivity threshold (higher censoring level), this observation suggests that the upper deposits of site FP17-01 represent GLOFs of particularly high magnitude.

An important observation is that none of the sediment cores show particularly inorganic-rich deposits in the last decade (the upper 1–2 cm), although the floodplain was clearly inundated due to Colonia GLOFs several times between 2008 and 2017 (Fig. 1c and Supplementary Fig. S1). Instead, the top of the records displays an apparent increase in LOI550 in the upper 10 cm (Figs. 3 and 6), suggesting that the magnitude of these GLOFs may have been too low to deposit large amounts of glacial material in the floodplain. This is supported by historical observations (Supplementary Table S1; Oportus, 1928; De Agostini, 1945) that indicate that only the pre-1960 GLOFs, which were of higher magnitude than those of the 21st century, were able to inundate the entire floodplain. Consequently, it is likely that, at the selected, relatively elevated, coring sites, the floodplain only registers the highest magnitude GLOFs.

Taken together, these observations suggest that the clastic fraction of the sediment cores collected in in the Valle Grande floodplain mostly represents high-magnitude glacial floods. The composite record (Fig. 6e) is therefore considered to represent the regional GLOF history, although precipitation-driven floods could also contribute to some extent to short-term changes in the sediment record, particularly at the base of the records.

5.4. Comparison with glacier and climate reconstructions

5.4.1. Relationship with glacier variability

The Baker River is predominantly fed by meltwater from outlet glaciers located along the eastern side of the NPI, superimposed on a baseflow from General Carrera Lake (Figs. 1a and 5). To examine the potential link between high-magnitude GLOF occurrence and changes in glacier mass-balance, the Valle Grande paleoflood record (Fig. 7a) was compared to reconstructions of Leones, Soler, Nef, Colonia, Arenales, and Arco glacier variability (Fig. 7b). It should be noted, however, that the available data on these glaciers is based on moraine and trimline dating and is therefore limited to reconstructions of maximum glacier advances or stabilization (Harrison and Winchester, 2000; Winchester et al., 2001; Glasser et al., 2002; Harrison et al., 2008; Nimick et al., 2016). These records are inherently discontinuous (moraine dating) and mostly cover short timescales (dendrochronology and lichenometry). Most of these records clearly show the latest advance during Neoglaciation V (Fig. 7b) but are too limited to reconstruct the late Holocene variations of these glaciers in detail.

The most complete glacier variability synthesis that covers the entire late Holocene is the timing of Neoglacial advances of Patagonian glaciers defined by Aniya (2013) (Fig. 7c). Results indicate that increased flooding coincides with Neoglacial advances III and V. Although the flood record shows a short-lived increase in flood activity c. 1.15 cal kyr BP, no high flood frequency period was registered during Neoglaciation IV. This neoglaciation, however, is not yet firmly confirmed (Aniya, 2013) and its existence is mostly based on chronological evidence from SPI glaciers, which are located c. two degrees of latitude to the south of Valle Grande. The existence of Neoglaciation IV in the NPI is only based on the analysis of two samples, including one of unknown origin, from the Soler Glacier valley (Aniya, 2013). It is therefore plausible that Neoglaciation IV only affected SPI glaciers, which would explain the discrepancy between our paleoflood record and the Aniya chronology for the 1.4–0.8 kyr time window.

An increase in high-magnitude GLOF occurrence during neoglaciations seems in contradiction with the apparent 21st century increase in GLOF frequency that is generally linked to increased glacier retreat and thinning rates (e.g., Iribarren Anacona et al., 2014; Wilson et al., 2018). It is however supported, on multi-decadal timescales, by oral history and ethnographic records that clearly describe that the Colonia GLOFs before the 1960s, i.e., when Colonia glacier was larger and thicker (Harrison and Winchester, 2000), were less frequent but of higher magnitude (Supplementary Table S1). It should also be noted that the GLOFs affecting the Valle Grande floodplain during the last century all initiated from ice-dammed lakes (Fig. 1a). In contrast to GLOF risks from moraine-dammed lakes, which increase during periods of glacier retreat (Benn and Evans, 2010), ice-dammed lakes generally form when drainage becomes blocked by advancing ice, leading to an increase in the risk of high-magnitude GLOF occurrence during periods of glacier growth (Round et al., 2017). In the Colonia valley for instance, the existence of the ice-dammed Cachet 2 and Arco lakes have been intermittent through time depending on the position of the Colonia Glacier (Nimick et al., 2016). A similar relation was suggested for the French Alps, where GLOFs originating from glacier-dammed lakes seem to have increased during the LIA (Vivian, 2001). GLOFs during periods of glacier advance could thus be less frequent but of higher magnitude than their modern counterparts. These results therefore suggest that the recent Cachet 2 GLOFs are relatively small compared to the high magnitude GLOFs that occurred during Neoglaciations III and V.

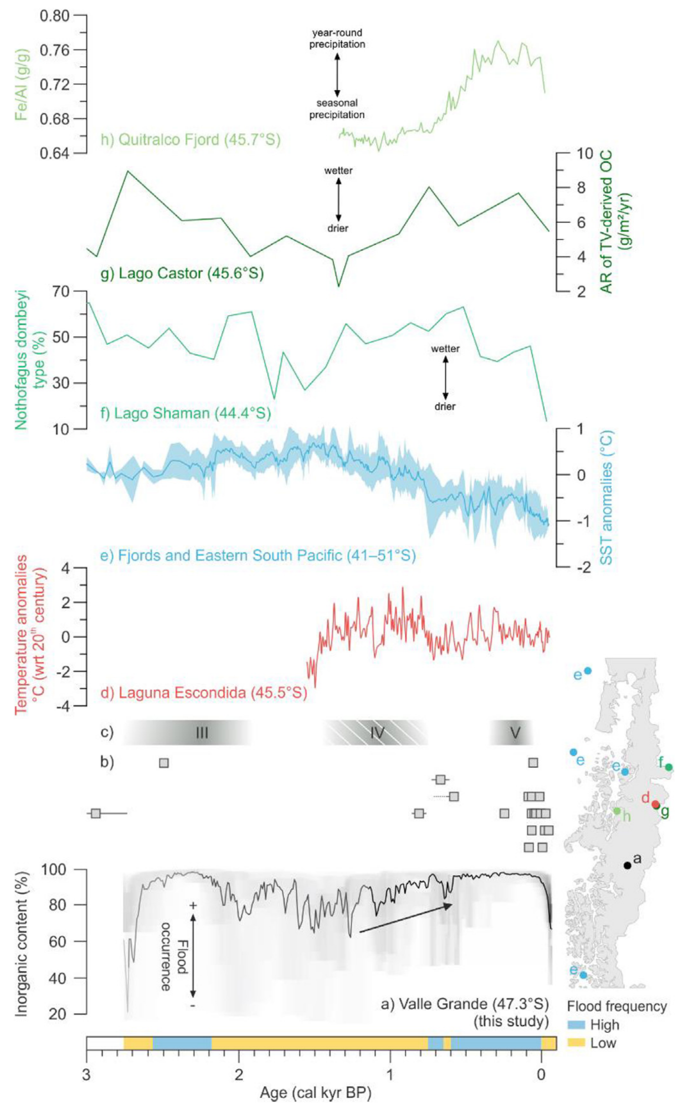

Fig. 7. Comparison of the composite Valle Grande flood record with regional glacier, temperature, and precipitation proxy records. (a) The composite high-magnitude flood frequency record from Valle Grande (this study). (b) Glacier advances of (from top to bottom, representing North to South) Leones (Harrison et al., 2008), Soler (Glasser et al., 2002), Nef (Winchester et al., 2001; Nimick et al., 2016), Colonia (Harrison and Winchester, 2000; Nimick et al., 2016), Arenales (Harrison and Winchester, 2000), and Arco (Harrison and Winchester, 2000). (c) Neoglacial advances of Patagonian glaciers (Aniya, 2013). Neoglaciation IV is represented using hatching since its existence is not firmly confirmed for the NPI (Aniya, 2013). (d) Reconstructed annual temperature anomalies derived from biogenic silica fluxes in Laguna Escondida (45.5°S) (Elbert et al., 2013). (e) Sea Surface Temperature (SST) anomalies derived from records along the southern Chilean margin from 41 to 51°S: GeoB3313 (41°S; Lamy et al., 2002), MD07-3093 (44°S; Collins et al., 2019), GeoB7186 (44°S; Mohtadi et al., 2007), and MD07-3124 (51°S; Caniupán et al., 2014). (f) Pollen record from Lago Shaman (44.4°S; de Porras et al., 2012). (g) Accumulation rate of terrestrial vegetation-derived organic carbon in Lago Castor (45.6°S; Fiers et al., 2019). (h) Fe/Al of core PC29A from Quitralco Fjord (45.7°S) used as a proxy for precipitation seasonality (Bertrand et al., 2014). The inset map indicates the location of the different proxy records presented in the figure.

5.4.2. Relationship with temperature

Due to the steep longitudinal climatic gradient that occurs in Patagonia (Garreaud et al., 2013), glacier fluctuations at the western and eastern sides of the NPI tend to differ. Indeed, several studies suggest that precipitation is the primary factor driving glacier dynamics on the western side of the icefield, whereas temperature plays a more important role on the eastern side (e.g., Warren and Sugden, 1993; Hulton et al., 1994; Aniya et al., 1997; Bertrand et al., 2012). As the Baker River drains most of the eastern side of the NPI, regional glacier dynamics is believed to be primarily controlled by ablation, which is in turn driven by (summer) temperature. Multi-decadal to millennial-scale changes in temperature could therefore have indirectly affected GLOF occurrence.

Terrestrial records of temperature are rather scarce around 45–48°S in Chilean Patagonia, and most cover shorter timescales (centuries) compared to our 2.75 kyr-long GLOF record (Neukom et al., 2011; Elbert et al., 2013). On the contrary, sea surface temperature (SST) reconstructions are more abundant and often date back thousands of years. SSTs are however less representative of the regional atmospheric temperature conditions that drive changes in ablation rates.

The regional reconstruction of annual air temperature anomalies derived from biogenic silica fluxes in Laguna Escondida (Elbert et al., 2013) shows a decrease in temperature during the last 750 years, coeval with the last period of increased flood occurrence (Fig. 7d). Likewise, the gridded summer surface air temperature reconstructions of Neukom et al. (2011) only cover the last 1000 years, but the grid cell encompassing the Valle Grande floodplain shows a significant drop in temperature around 0.55 cal kyr BP that corresponds in timing to the shift towards increased flooding during the last 600 years.

Comparison with SST reconstructions along the southern Chilean margin (Lamy et al., 2002; Mohtadi et al., 2007; Sepúlveda et al., 2009; Caniupán et al., 2014; Collins et al., 2019) shows that, in general, increased flooding occurs during periods of lower-than-average SST (Fig. 7e). In particular, the cooling transition between 0.90 and 0.60 cal kyr BP strongly coincides with a transition towards increased flood occurrence. Higher flood occurrence at 2.57–2.17 cal kyr BP also corresponds to lower-than-average SST values before 2.2 cal kyr BP (Fig. 7e). These comparisons therefore tend to show that the frequency of high-magnitude GLOFs tends to increase during colder periods, which may have been responsible for NPI glacier advances during Neoglaciations III and V.

5.4.3. *Relationship with precipitation*

As mentioned above, the influence of precipitation on flood occurrence in the Baker River basin could be two-fold. First, extreme precipitation events could induce flooding of the Baker River by direct run-off. The magnitude of these flooding events however appears much smaller than GLOFS, and their signature in our Valle Grande sediment cores is probably not as significant as high-magnitude GLOFs. Second, long-term increases in precipitation could contribute to regional glacier advances and therefore be partly responsible for the glacier advance – frequent high-magnitude GLOF relationship put forward in section 5.4.1.

Late Holocene flood reconstructions are almost inexistent in Chilean Patagonia and the only existing precipitation reconstructions in the Baker watershed are based on pollen records (Villa-Martínez et al., 2012; McCulloch et al., 2017). We therefore compared the Valle Grande paleoflood record to previously published precipitation proxy records to assess the relation between centennial-to-millennial variations in precipitation and high-magnitude flood occurrence. For the last 3000 years, these pollen records are dominated by *Nothofagus dombeyi*-type, indicating the persistence of humid-temperate conditions, without any significant change. The only records that do show variations during the late Holocene are located 2–3° of latitude to the north. The pollen record of Lago Shaman (de Porras et al., 2012, Fig. 7f), for example, shows high-amplitude variability during the late Holocene, likely because it is located near the forest-steppe ecotone. In general, the periods of high flood occurrence at 2.57–2.17 cal kyr BP and at 0.75–0 cal kyr BP coincide with wetter conditions inferred from the pollen assemblages (Fig. 7f). There is, however, a mismatch during the last 500 yrs, during which floods are frequent when the Lago Shaman record indicates a transition towards drier conditions. In contrast, the Lago Castor sediment record (Fiers et al., 2019) shows increased precipitation from 2.8 to 2.2 cal kyr BP but also during the last 800 years (Fig. 7g). These two wet periods correspond remarkably well to periods of high flood occurrence derived from the Valle Grande sediment cores. Finally, the increase in year-round precipitation during the last 800 years is also clearly marked in the Quitralco Fjord sediment record on the western side of the NPI (Fig. 7h; Bertrand et al., 2014). These comparisons therefore suggest that high-magnitude GLOFs are more frequent during periods of higher year-round precipitation.

5.5. *Link between GLOF occurrence and climate and glacier variability*

The results presented above suggest that high-magnitude GLOFs in Valle Grande were more frequent during Neoglaciations III (2.8–2.0 cal kyr BP) and V (17^{th}–19^{th} centuries). These two periods are characterized by lower-than-average temperatures and wetter conditions, suggesting a link between climate and glacier variability, i.e., cold and wetter conditions result in a positive glacier mass balance. Although flooding caused by extreme precipitation can lead to the deposition of clastic material, the majority of the flood deposits evident in the sediment cores from Valle Grande likely represent high-magnitude GLOFs that increased in frequency during glacier advances. These results do not contradict the observation that the 21^{st} century increase in Cachet 2 GLOFs coincides with glacier retreat, but they suggest that, on longer timescales, GLOFs are of higher magnitude when glaciers are larger and thicker. This relation between larger glaciers and increase in the frequency of high-magnitude GLOFs during the late Holocene is supported by (1) historical information that indicates the presence of high-magnitude GLOFs during the first half of the 20^{th} century; (2) the fact that larger glaciers are able to restrain larger water bodies, which in turn result in higher magnitude GLOFs when the dam fails; and (3) similar observations made on shorter timescales in the European Alps and in the Chinese Karakoram (Vivian et al., 2001; Round et al., 2017). Although the frequency of GLOFs in the Baker River watershed is currently high, the magnitude of these events appears significantly lower than those that occurred during periods of glacier advance during the late Holocene. Our results therefore suggest that the probability that a high-magnitude GLOF occurs decreases as glaciers thin and retreat.

6. Conclusions

The Valle Grande floodplain contains a continuous record of flood activity during the last 2.75 kyr. Our results show that elevation in the floodplain plays a major role in controlling the sediment infill. Sites at low elevation are dominated by relatively homogeneous clastic deposits and are therefore not suited for flood reconstruction. Sites at higher elevations, on the other hand, display channel-fill sequences where autochthonous organic-rich sedimentation alternates with flood deposits (clastics). These sites are the most promising in terms of flood archives. They register high-magnitude floods without being affected by minor events. Sedimentological and historical information suggest that the majority of the flood deposits recorded in Valle Grande represent high-magnitude GLOFs.

Our results indicate that high-magnitude GLOFs occurred intermittently over the last 2.75 kyr and that their frequency was particularly high between c. 2.57–2.17 cal kyr BP, and c. 0.75–0 cal kyr BP. These two periods of high flood frequency correspond to Neoglacial advances III and V, suggesting a strong relationship between glacier advance and GLOF occurrence. Since these glacier advances seem to result from lower-than-average temperatures and wetter conditions, our results suggest a close, indirect, link between climate variability and GLOF occurrence. The recent period of increased flooding between 0.75 and 0 cal kyr BP specifically coincides with the colder and wetter conditions that resulted in the advance of Patagonian glaciers in the 15th–19th centuries.

Overall, our study suggests that high-magnitude GLOFs from eastern NPI glaciers occur more frequently when glaciers are larger and thicker. This relation likely reflects the ability of larger glaciers to form larger and stronger ice dams, which are in turn able to hold larger lakes. Although lake outbursts may be less frequent under these conditions, our results suggest that when they occur, they generate higher magnitude floods. These results do not contradict the apparent increase in GLOF frequency during the last decades but they suggest that, on multi-centennial timescales, GLOF are of higher magnitude when glaciers are larger. These results emphasize the need to consider different timescales when researching natural hazards, and they support the use of geological archives to complement monitoring data for proper flood hazard assessment. Based on these results, we suggest that the probability that a high-magnitude GLOF occurs decreases as glaciers thin and retreat.

Declaration of competing interest

The authors declare that they have no known competing financial interests or personal relationships that could have appeared to influence the work reported in this paper.

Acknowledgements

We thank Eleonora Crescenzi Lanna, Loïc Piret, and Francois De Vleeschouwer for assistance in the field. Elie Verleyen and Wim Vyverman are thanked for providing the Russian corer. We are also grateful to Olaf Wuendrich for shipping samples and equipment back to Belgium. We would like to thank Horacio Parrague, Andrés Rivera, and Paulina Rojas for providing the aerial photographs shown in Fig. 1. Atun Zawadzki is thanked for conducting the ^{210}Pb analyses. We are grateful to Benjamin Amann, Dawei Liu and Loïc Piret for their valuable input. We thank Varyl Thorndycraft and one anonymous reviewer for providing comments that improved an earlier version of this manuscript. The research presented here was funded by the Flemish Research Foundation (FWO, Belgium; project Paleo-GLOFs G0D7916N).

Appendix A. Supplementary data

Supplementary data to this article can be found online at https://doi.org/10.1016/j.quascirev.2020.106572.

References

Alvarez-Garreton, C., Mendoza, P.A., Boisier, J.P., Addor, N., Galleguillos, M., Zambrano-Bigiarini, M., Lara, A., Puelma, C., Cortes, G., Garreaud, R., McPhee, J., Ayala, A., 2018. The CAMELS-CL dataset: catchment attributes and meteorology for large sample studies – Chile dataset. Hydrol. Earth Syst. Sci. 22, 5817–5846.
Aniya, M., 1995. Holocene glacial chronology in Patagonia: tyndall and upsala glaciers. Arctic Antarct. Alpine Res. 27, 311–322.
Aniya, M., 1996. Holocene variations of ameghino glacier, southern Patagonia. Holocene 6, 247–252.
Aniya, M., Sato, H., Naruse, R., Skvarca, P., Casassa, G., 1997. Recent glacier variations in the south patagonian icefield, south America. Arct. Alp. Res. 29, 1–12.
Aniya, M., 2013. Holocene glaciations of hielo patagónico (Patagonia icefield), south America: a brief review. Geochem. J. 47, 97–105.
Aniya, M., 2017. Glacier variations of hielo patagónico norte, Chile, over 70 years from 1945 to 2015. Bull. Glaciol. Res. 35, 19–38.
Bastianon, E., Bertoldi, W., Dussaillant, A., 2012. Glacial-lake Outburst Flood Effects on Colonia River Morphology, Chilean Patagonia. River Flow 2012. CRC Press, pp. 573–579.
Benito, G., Thorndycraft, V.R., 2020. Catastrophic glacial-Lake Outburst flooding of the patagonian ice sheet. Earth Sci. Rev. 200, 102996.
Benito, G., Thorndycraft, V.R., Machado, M.J., Sancho, C., Dussaillant, A., Meier, C.I., 2014. Magnitud y frecuencia de inundaciones Holocenas generadas por vaciamiento de lagos glaciares en el Rio Baker, Campo de Hielo, Patagonico Norte, Chile. In: Schnabel, S., Gutiérrez, Á.G. (Eds.), Sociedad Española de Geomorfología. Cáceres, Spain, pp. 24–27.
Benn, D.I., Evans, D.J.A., 2010. Glaciers and Glaciation, second ed. Hodder education, London, p. 802.
Bertrand, S., Hughen, K.A., Lamy, F., Stuut, J.-B.W., Torrejón, F., Lange, C.B., 2012. Precipitation as the main driver of neoglacial fluctuations of gualas glacier, northern patagonian icefield. Clim. Past 8, 519–534.
Bertrand, S., Hughen, K., Sepúlveda, J., Pantoja, S., 2014. Late Holocene covariability of the southern westerlies and sea surface temperature in northern Chilean Patagonia. Quat. Sci. Rev. 105, 195–208.
Blaauw, M., 2010. Methods and code for 'classical' age-modelling of radiocarbon sequences. Quat. Geochronol. 5, 512–518.
Blaauw, M., Christen, J.A., 2011. Flexible paleoclimate age-depth models using an autoregressive gamma process. Bayesian Analysis 6, 457–474.
Caniupán, M., Lamy, F., Lange, C.B., Kaiser, J., Kilian, R., Arz, H.W., León, T., Mollenhauser, G., Sandoval, S., De Pol-Holz, R., Pantoja, S., Wellner, J., Tiedemann, R., 2014. Holocene sea-surface temperature variability in the Chilean fjord region. Quat. Res. 82, 342–353.
Carrivick, J.L., Quincey, D.J., 2014. Progressive increase in number and volume of ice-marginal lakes on the western margin of the Greenland Ice Sheet. Global Planet. Change 116, 156–163.
Carrivick, J.L., Tweed, F.S., 2016. A global assessment of the societal impacts of glacier outburst floods. Global Planet. Change 144, 1–16.
Collins, J.A., Lamy, F., Kaiser, J., Ruggieri, N., Henkel, S., De Pol-Holz, R., Garreaud, R., Arz, H.W., 2019. Centennial-scale SE Pacific sea surface temperature variability over the past 2,300 years. Paleoceanography and Paleoclimatology 34, 336–352.
Davies, B.J., Darvill, C.M., Lovell, H., Bendle, J.M., Dowdeswell, J.A., Fabel, D., García, J.-L., Geiger, A., Glasser, N.F., Gheorghiu, D.M., Harrison, S., Hein, A.S., Kaplan, M.R., Martin, J.R.V., Mendelova, M., Palmer, A., Pelto, M., Rodés, Á., Sagredo, E.A., Smedley, R.K., Smellie, J.L., Thorndycraft, V.R., 2020. The evolution of the Patagonian Ice Sheet from 35 ka to the present day (PATICE). Earth-Sci. Rev. 204, 103152.
Davies, B.J., Glasser, N.F., 2012. Accelerating shrinkage of patagonian glaciers from the little ice age (~AD 1870) to 2011. J. Glaciol. 58 (212), 1063–1084.
De Agostini, A.S.S., 1945. Andes Patagónicos, Viajes de exploración a la Cordillera Patagónica Austral. Segunda edición aumentada y corregida, Buenos Aires, p. 436.
De Porras, M.E., Maldonado, A., Abarzúa, A.M., Cáardenas, M.L., Francois, J.P., Martel-Cea, A., Stern, C.R., Méndez, C., Reyes, O., 2012. Postglacial vegetation, fire and climate dynamics at central Chilean Patagonia (lake shaman, 44°S). Quat. Sci. Rev. 50, 71–85.
Dieras, P.L., Constantine, J.A., Hales, T.C., Piégay, H., Riquier, J., 2013. The role of oxbow lakes in the off-channel storage of bed material along the Ain River, France. Geomorphology 188, 110–119.
Dussaillant, A., Benito, G., Buytaert, W., Carling, P., Meier, C., Espinoza, F., 2010. Repeated glacial-lake outburst floods in Patagonia: an increasing hazard? Nat. Hazards 54, 469–481. https://doi.org/10.1007/s11069-009-9479-8.
Dussaillant, A., Buytaert, W., Meier, C., Espinoza, F., 2012. Hydrological regime of remote catchments with extreme gradients under accelerated change: the Baker basin in Patagonia. Hydrol. Sci. J. 57 (8), 1530–1542. https://doi.org/10.1080/02626667.2012.726993.
Elbert, J., Wartenburger, R., von Gunten, L., Urrutia, R., Fischer, D., Fujak, M., Hamann, Y., Greber, N.D., Grosjean, M., 2013. Late Holocene air temperature variability reconstructed from the sediments of Laguna Escondida, Patagonia, Chile (45°30'S). Palaeogeogr. Palaeoclimatol. Palaeoecol. 369, 482–492.
Fick, S.E., Hijmans, R.J., 2017. WorldClim 2: new 1-km spatial resolution climate surfaces for global land areas. Int. J. Climatol. 37, 4302–4315.
Fiers, G., Bertrand, S., van Daele, M., Granon, E., Reid, B., Vandoorne, W., De Batist, M., 2019. Hydroclimate variability of northern Chilean Patagonia during the last 20 kyr inferred from the bulk organic geochemistry of Lago Castor sediments (45°S). Quat. Sci. Rev. 204, 105–118.
Friesen, B.A., Cole, C.J., Nimick, D.A., Wilson, E.M., Fahey, M.J., McGrath, D., Leidich, J., 2015. Using satellite images to monitor lake outburst floods—Lago Cachet Dos drainage, Chile. U.S. Geological Survey Scientific Investigations Map 3322. https://doi.org/10.3133/sim3322 scale 1:15,000.
Fuller, I.C., Macklin, M.G., Toonen, W.H.J., Holt, K.A., 2018. Storm-generated Holocene and historical floods in the manawatu river, New Zealand. Geomorphology 310, 102–124.
Fuller, I.C., Macklin, M.G., Toonen, W.H.J., Turner, J., Norton, K., 2019. A 2000 year record of palaeofloods in a volcanically-reset catchment: whanganui River, New Zealand. Global Planet. Change 181.
Garreaud, R., Lopez, P., Minvielle, M., Rojas, M., 2013. Large-scale control on the Patagonian climate. J. Clim. 26, 215–230.

Glasser, N.F., Hambrey, M.J., Aniya, M., 2002. An advance of Soler Glacier, north patagonian icefield at c. AD 1222–1342. Holocene 12 (1), 113–120.
Glasser, N.F., Jansson, K.N., Duller, G.A.T., Singarayer, J., Holloway, M., Harrison, S., 2016. Glacial lake drainage in Patagonia (13-8 kyr) and response of the adjacent Pacific Ocean. Sci. Rep. 6, 21064.
Harrison, S., Winchester, V., 2000. Nineteenth- and twentieth century glacier fluctuations and climate implications in the Arco and Colonia valleys, Hielo Patagónico Norte, Chile. Arctic Antarct. Alpine Res. 32, 55–63.
Harrison, J., Heijnis, H., Caprarelli, G., 2003. Historical pollution variability from abandoned mine sites, greater blue mountains world heritage area, new south wales, Australia. Environ. Geol. 43, 680–687.
Harrison, S., Glasser, N., Winchester, V., Haresign, E., Warren, C., Duller, G.A.T., Bailey, R., Ivy-Ochs, S., Jansson, K., Kubik, P., 2008. Glaciar León, Chilean Patagonia: late-Holocene chronology and geomorphology. Holocene 18 (4), 643–652.
Harrison, S., Kargel, J.S., Huggel, C., Reynolds, J., Shugar, D.H., Betts, R.A., Emmer, A., Glasser, N., Haritashya, U.K., Klimeš, J., Reinhardt, L., Schaub, Y., Wiltshire, A., Regmi, D., Vilímek, V., 2018. Climate change and the global pattern of moraine-dammed glacial lake outburst floods. Cryosphere 12, 1195–1209.
Heiri, O., Lotter, A.F., Lemcke, G., 2001. Loss on ignition as a method for estimating organic and carbonate content in sediments: reproducibility and comparability of results. J. Paleolimnol. 25, 101–110.
Hogg, A.G., Hua, Q., Blackwell, P.G., Niu, M., Buck, C.E., Guilderson, T.P., Heaton, T.J., Palmer, J.G., Reimer, P.J., Reimer, R.W., Turney, C.S.M., Zimmerman, S.R.H., 2013. SHCal13 southern hemisphere calibration, 0-50,000 years cal BP. Radiocarbon 55, 1889–1903.
Hooke, J.M., 1995. River channel adjustment to meander cutoffs on the river Bollin and river Dane, northwest England. Geomorphology 14, 235–253.
Hulton, N., Sugden, D., Payne, A., Clapperton, C., 1994. Glacier modeling and the climate of Patagonia during the last glacial maximum. Quat. Res. 42, 1–19.
IPCC, 2019. IPCC Special Report on the Ocean and Cryosphere in a Changing Climate. Intergovernmental Panel on Climate Change, p. 765.
Iribarren Anacona, P., Mackintosh, A., Norton, K.P., 2014. Hazardous processes and events from glacier and permafrost areas: lessons from the Chilean and Argentinean Andes. Earth Surf. Process. Landforms 40, 2–21.
Ishii, Y., Hori, K., Momohara, A., 2017. Middle to late Holocene flood activity estimated from loss on ignition of peat in the Ishikari lowland, northern Japan. Global Planet. Change 153, 1–15.
Jacquet, J., McCoy, S.W., McGrath, D., Nimick, D.A., Fahey, M., O'kuinghttons, J., Friesen, B.A., Leidlich, J., 2017. Hydrologic and geomorphic changes resulting from episodic glacial lake outburst floods: rio Colonia, Patagonia, Chile. Geophys. Res. Lett. 44, 854–864. https://doi.org/10.1002/2016GL071374.
Jones, A.F., Macklin, M.G., Brewer, P.A., 2012. A geochemical record of flooding on the upper River Severn, UK, during the last 3750 years. Geomorphology 179, 89–105.
Lamy, F., Rühlemann, C., Hebbeln, D., Wefer, G., 2002. High- and low-latitude climate control on the position of the southern Peru-Chile Current during the Holocene. Paleoceanography 17. https://doi.org/10.1029/2001PA000727.
Lara, A., Bahamondez, A., González-Reyes, A., Muñoz, A.A., Cuq, E., Ruiz-Gómez, C., 2015. Reconstructing streamflow variation of the Baker river from tree-rings in northern Patagonia since 1765. J. Hydrol. 529 (2), 511–523.
Lenaerts, J.T.M., Van Den Broeke, M.R., Van Wessem, J.M., Jan Van Den Berg, W., 2014. Extreme precipitation and climate gradients in Patagonia revealed by high-resolution regional atmospheric climate modeling. J. Clim. 33, 4607–4621.
Lintern, A., Leahy, P.J., Zawadzki, A., Gadd, P., Heijnis, H., Jacobsen, G., Connor, S., Deletic, A., McCarthy, D.T., 2016. Sediment cores as archives of historical changes in floodplain lake hydrology. Sci. Total Environ. 544, 1008–1019.
Masiokas, M.H., Rivera, A., Espizua, L.E., Villalba, R., Delgado, S., Carlos Aravena, J., 2009. Glacier fluctuations in extratropical South America during the past 1000 years. Palaeogeogr. Palaeoclimatol. Palaeoecol. 281, 242–268.
Mauquoy, D., Van Geel, B., Blaauw, M., Speranza, A., van der Plicht, J., 2004. Changes in solar activity and Holocene climatic shifts derived from 14C wiggle-match dated peat deposits. Holocene 14, 45–52.
McCulloch, R.D., Figuerero Torres, M.J., Mengoni Goñalons, G.L., Barclay, R., Mansilla, C., 2017. A Holocene record of environmental change from Río Zeballos, central Patagonia. Holocene 27 (7), 941–950.
Mercer, J.H., 1982. Holocene glacier variations in southern South America. Striae 18, 35–40.
Minderhoud, P.S.J., Cohen, K.M., Toonen, W.H.J., Erkens, G., Hoek, W.Z., 2016. Improving age-depth models of fluvio-lacustrine deposits using sedimentary proxies for accumulation rates. Quat. Geochronol. 33, 35–45.
Mohtadi, M., Romero, O.E., Kaiser, J., Hebbeln, D., 2007. Cooling of the southern high latitudes during the Medieval Period and its effect on ENSO. Quat. Sci. Rev. 26, 1055–1066.
Nanson, G.C., Beach, H.F., 1977. Forest succession and sedimentation on a meandering-river floodplain, northeast British Columbia, Canada. J. Biogeogr. 4, 229–251.
Neukom, R., Luterbacher, J., Villalba, R., Küttel, M., Frank, D., Jones, P.D., Grosjean, M., Wanner, H., Aravena, J.-C., Black, D.E., Christie, D.A., D'Arrigo, R., Lara, A., Morales, M., Soliz-Gamboa, C., Srur, A., Urrutia, R., von Gunten, L., 2011. Multiproxy summer and winter surface air temperature field reconstructions for southern South America covering the past centuries. Clim. Dynam. 37, 35–51.
Nimick, D.A., McGrath, D., Mahan, S.A., Friesen, B.A., Leidich, J., 2016. Latest pleistocene and Holocene glacial events in the Colonia valley, northern patagonian icefield, southern Chile. J. Quat. Sci. 31 (6), 551–564.
Oportus, C., 1928. Informe sobre el problema de colonización de la zona del Río Baker. Republica de Chile-Ministerio de Fomento, p. 106.
Paine, J.L., Rowan, J.S., Werritty, A., 2002. Reconstructing historic floods using sediment from embanked flood plains: a case study of the river tay in scotland. The structure, function and management implications of fluvial sedimentary systems. In: Proceedings of an International Symposium at Alice Springs, Australia, September 2002, vol. 276. IAHS Publ, p. 2002.
Paul, F., Kääb, A., Haeberli, W., 2007. Recent glacier changes in the Alps observed by satellite: consequences for future monitoring strategies. Global Planet. Change 56, 111–122.
Prakash, C., Nagarajan, R., 2018. Glacial lake changes and outburst flood hazard in Chandra basin, North-Western Indian Himalaya. Geomatics, Nat. Hazards Risk 9, 337–355.
Quiroga, E., Ortiz, P., Gerdes, D., Reid, B., Villagran, S., Quiñones, R., 2011. Organic enrichment and structure of macrobenthic communities in the glacial Baker fjord, Northern Patagonia, Chile. J. Mar. Biol. Assoc. U. K. 92 (1), 73–83.
Round, V., Leinss, S., Huss, M., Haemmig, C., Hajnsek, I., 2017. Surge dynamics and Lake outbursts of kyagar glacier, Karakoram. Cryosphere 11, 723–739.
Saint-Laurent, D., Lavoie, L., Drouin, A., St-Laurent, J., Ghaleb, B., 2010. Floodplain sedimentation rates, soil properties and recent flood history in southern Québec. Global Planet. Change 70, 76–91.
Sepúlveda, J., Pantoja, S., Hughen, K.A., Bertrand, S., Figueroa, D., León, T., Drenzek, J., Lange, C., 2009. Late Holocene sea-surface temperature and precipitation variability in northern Patagonia, Chile. Quat. Res. 72, 400–409.
Sernageomin, 2003. Mapa geologico de Chile versión digital, scale 1/1.000.000.
Tanaka, K., 1980. Geographic Contribution to a Periglacial Study of the Hielo Patagonico Norte with Special Reference to the Glacial Outburst Originated from Glacier-Dammed Lago Arco, Chilean Patagonia. Centre Co Ltd, Tokyo, p. 97.
Toonen, W.H.J., Kleinhans, M.G., Cohen, K.M., 2012. Sedimentary architecture of abandoned channel fills. Earth Surf. Process. Landforms 37, 459–472.
Toonen, W.H.J., Winkels, T.G., Cohen, K.M., Prins, M.A., Middelkoop, H., 2015. Lower Rhine historical flood magnitudes of the last 450 years reproduced from grain-size measurements of flood deposits using End Member Modelling. Catena 130, 69–81.
Thorndycraft, V.R., Bendle, J.M., Benito, G., Davies, B.J., Sancho, C., Palmer, A.P., Fabel, D., Medialdea, A., Martin, J.R.V., 2019. Glacial lake evolution and Atlantic-Pacific drainage reversals during deglaciation of the Patagonian Ice Sheet. Quat. Sci. Rev. 203, 102–127.
Turner, K.J., Fogwill, C.J., McCulloch, R.D., Sugden, D.E., 2005. Deglaciation of the eastern flank of the North Patagonian Icefield and associated continental-scale lake diversions. Geogr. Ann. 87A, 363–374.
Ulloa, H., Mazzorana, B., Batalla, R.J., Jullian, C., Iribarren-Anacona, P., Barrientos, G., Reid, B., Oyarzun, C., Schaefer, M., Iroumé, A., 2018. Morphological characterization of a highly-dynamic fluvial landscape: the River Baker (Chilean Patagonia). J. S. Am. Earth Sci. 86, 1–14.
Villa-Martínez, R., Moreno, P.I., Valenzuela, M.A., 2012. Deglacial and postglacial vegetation changes on the Eastern slopes of the central Patagonian Andes (47 °S). Quat. Sci. Rev. 32, 86–99.
Vivian, R., 2001. Des Glaciers du Faucigny aux Glaciers de Mont Blanc. La Fontaine de Siloe, Montmelian.
Wang, W., Yao, T., Yang, X., 2011. Variations of glacial lakes and glaciers in the Boshula mountain range, southeast Tibet, from the 1970s to 2009. Annuals of Glaciology 52, 9–17.
Warren, C.R., Sugden, D.E., 1993. The Patagonian Icefields: a glaciological review. Arct. Alp. Res. 25, 316–331.
Wessel, B., Huber, M., Wohlfart, C., Marschalk, U., Kosmann, D., Roth, A., 2018. Accuracy assessment of the global TanDEM-X digital elevation model with GPS data. ISPRS J. Photogrammetry Remote Sens. 139, 171–182.
Wilson, R., Glasser, N.F., Reynolds, J.M., Harrison, S., Anacona, P.I., Schaefer, M., Shannon, S., 2018. Glacial lakes of the central and patagonian Andes. Global Planet. Change 162, 275–291.
Winchester, V., Harrison, S., 2000. Dendrochronology and lichenometry: colonization, growth rate and dating of geomorphological events on the east side of the North Patagonian Icefield, Chile. Geomorphology 34, 181–194.
Winchester, V., Harrison, S., Warren, C.R., 2001. Recent retreat glaciar Nef, Chilean Patagonia, dated by lichenometry and dendrochronology. Arctic Antarct. Alpine Res. 33, 266–273.
Zhang, G., Bolch, T., Allen, S., Linsbauer, A., Chen, W., Wang, W., 2019. Glacial lake evolution and glacier-lake interactions in the Poiqu River basin, central Himalaya, 1964–2017. J. Glaciol. 65, 347–365.